

D26  
N79-24027

## ENVIRONMENTAL INTERACTION IMPLICATIONS FOR LARGE SPACE SYSTEMS

E. Miller, W. Fischbein, M. Stauber, P. Suh  
Grumman Aerospace Corporation

### ABSTRACT

Large Space Systems (LSS) comprise a new class of spacecraft, the design and performance of which may be seriously affected by a variety of environmental interactions.

In addition to dimensions which are orders of a magnitude larger than those of conventional spacecraft, most LSS are characterized by low density structures, extensive dielectric surfaces and composite structural elements. Many LSS also require multikilowatt or megawatt power systems, which might operate at multikilovolt levels. Perhaps most significant is that most of these advanced systems must operate efficiently for 10 to 30 years with little or no maintenance.

This paper addresses the special concerns associated with spacecraft charging and plasma interactions from the LSS designer's viewpoint. Survivability of these systems under combined solar U.V., particle radiation and repeated electrical discharges is of primary importance. Additional questions regard the character of electrical discharges over very large areas, the effects of high current/voltage systems and magnitude of induced structural disturbances.

Incorporation of large scale charge controls and complicated electrical and structural interactions could impose difficult design requirements and have a major impact on LSS costs. Worst-case estimates are made, and possible design/performance impacts assessed for LSS environmental interactions of major concern.

A concept is described for a large scale experiment platform which utilizes space structure demonstration articles presently under study by the Air Force and NASA. These platforms could provide several thousand square meters of test area, with maximum dimensions up to one kilometer.

Accelerated charge/discharge, induced avalanche and plasma power loss experiments might be configured for low earth orbit, and the free-flyer test platform retrieved after several months for analysis of combined environmental effects. Additional instrumentation could be installed, the platform boosted to geosynchronous orbit to measure large scale plasma characteristics and spacecraft interactions, and test samples retrieved with a manned orbit transfer vehicle after long-term exposure.

### INTRODUCTION

The Space Shuttle will open a new era of space transportation in the early 1980's. A multitude of long duration, complex, multifunction missions will be possible with the unique capabilities of the Space Transportation System (STS). Many of the advanced missions considered for the next two decades will require a new generation of spacecraft, called Large Space Systems (LSS).

Some of the LSS concepts, devised for a variety of applications, are illustrated in Figure 1. The LSS of the 1980's will be orders of magnitude larger than anything launched to date. Most will be constructed in space using materials and support machinery transported by the STS. By the 1990's, much larger Solar Power System demonstration articles, second or third generation LSS, might be flown.

Although designed for a wide variety of missions, the basic characteristics of most unmanned LSS are quite similar. Spaceborne radars, communication and scientific platforms and solar power demonstration articles are large, low density structures which generally make extensive use of dielectric and composite materials. Exposed surface areas for these systems range from thousands to millions of square meters. Also, several missions require multikilowatt to megawatt electrical power sources and could operate at multikilovolt levels.

Numerous analytical, manufacturing and test methods must be developed to deal with these huge structures, high power and voltage levels and novel construction and deployment techniques. One of the greatest challenges facing the LSS designer, however, is to achieve a reliable, efficient system which can survive the space environment, with little or no maintenance for 10 to 30 years.

The need for long-term environmental effects data on LSS candidate materials is well known. Some laboratory tests have already begun and flight experiments (SCATHA, LDEF) are scheduled for the near future. The compounding effects of electrostatic charging and repeated electrical discharges on materials and components and structural and electrical interactions with the space plasma could have a serious impact on the design, performance and economic viability of many LSS.

A program was initiated by Grumman last year to assess the impact of environmental interactions on the LSS under study. This combined engineering/research effort includes modeling of coupling mechanisms, identification of most probable trouble spots, nominal and worst-case estimates of environmental effects and alternate design approaches to minimize or eliminate damaging effects. Some of the results of these studies are described below.

#### DESCRIPTION OF-TYPICAL LARGE SPACE SYSTEMS

Several LSS programs have been conducted by Grumman during the past few years. Conceptual and preliminary designs have been developed for solar power satellites, space stations, space-based radars, multifunction communication and surveillance platforms, space construction platforms and large space structure demonstration articles. Two such systems, designed for widely different missions, are the Space Based Radar (SBR) and Solar Power Satellite (SPS) Demonstration Article.

#### SBR

The general arrangement of a typical SBR is shown in Figure 2. This system employs a unique, deployable wire wheel antenna which can be stowed in and deployed from the shuttle in diameters up to 300 meters.

The antenna is attached to and supported by a drum that is the basic structure at the lower end. This drum also provides mounting surfaces for communications antennas, the lower systems package (LSP), the lower attitude control thrusters and the mast canister. Attached to the upper end of a deployable mast is the upper systems package (USP) which provides mounting surfaces for the antenna feed, upper thrusters and solar or nuclear power source.

The phased-array antenna is supported by a graphite/epoxy compression rim assembly which, in turn, is supported by spring-tensioned fore and aft stays (graphite/epoxy strips). The phased-array antenna is made of gore panel assemblies that lie in the plane of the rim and are spring-tensioned between the rim and drum. The compression rim assembly is a polygon composed of thinwall tubes; the number and length depends on the deployed diameter.

The triangular antenna array gore assemblies, shown in Figure 3, are made in sections and spliced together by circumferential mini-hinged beams that provide the required interlayer spacing. For the space-fed phased array, the triple layer panels consist of ground-side and feed-side antenna planes located one quarter wave-length from the ground plane.

The antenna planes consist of frame-mounted subarrays shown in Figure 4. The frames are assembled edge-to-edge in an axisymmetric array of rows and columns within the bounds of the gore section. Each frame is a square structure made of 2.5 mil aluminum. The sub-arrays, dipoles and feed lines are made of 0.25 mil copper, on 1 mil H-film substrate.

The ground plane consists of a 2.5 mil pierced aluminum sheet. The resulting mesh sections are bounded by radial edge tapes and reinforced with transverse aluminum battens.

Solid state RF amplifiers and digital electronics are mounted on the ground plane. These are powered from upper and lower antenna planes at +180 vdc and -10 vdc respectively. The electrical network, distributed throughout the antenna, carries about 90% of the total generated power to several hundred thousand electronic modules.

All antenna and ground plane surfaces may be covered with a thermal control coating to minimize temperature gradients throughout the array. Electrically conductive coatings could be used on the ground plane, but non-conductive coatings would be used on the antenna planes to permit proper operation of the dipoles.

The LSP drum is fabricated of aluminum alloy in a thin skin, cylindrical configuration. The USP is also fabricated of aluminum alloy. The nuclear reactor mast or solar array support structure (with drive motors) mounts to the upper frame of the USP. Up to 100 kilowatts of power is provided to the sub-systems and phased array modules.

Depending on system size, jet or ion thrusters are used for attitude control. Thrusters mounted on the LSP provide stationkeeping, roll control, and

part of the pitch and yaw control. Additional thrusters are mounted on the USP to complete pitch and yaw control.

Active or passive versions of the deployable wire wheel antenna can be used for many different missions. Grumman has emphasized the phased array approach for SBR, and detailed lightweight gore designs and models have been developed for these systems. Reflector and bootlace lens antennas have also been designed for radiometry and communications systems.

#### SPS Demonstration Article

Feasibility and conceptual design studies conducted over the past few years have shown that the SPS is an attractive power source alternative for the twenty first century. Further technology development is being encouraged, and it is likely that some form of SPS technology verification spacecraft will be flown in the 1990's.

The relative scales of these SPS test articles can be appreciated from Figure 5. Here, some of the growth possibilities leading to the full-scale SPS are illustrated. Note that even modestly sized demonstrations systems are from ten to several hundred times larger than the largest photovoltaic system presently being considered for the early 1980's - - a 50 kilowatt array for the LEO power module.

Several photovoltaic SPS concepts are being studied including planar and concentrator arrays, silicon, gallium arsenide and other solar cells. The structural arrangement of a typical concentrator SPS is shown in Figure 6. Solar cell blanket and concentrator support trusses are of aluminum or composite material, constructed from smaller, one-meter beams which are automatically fabricated in space. The slotted waveguide antenna is made of aluminum or metallized composites and includes thousands or millions of DC-RF converters.

Cross sections of advanced solar cell blankets which might be used for the SPS are shown in Figure 7. Compared to current technology, SPS solar cell blankets will be much thinner and lighter. Glass or plastics might be used for substrates or continuous cell covers. Solar cells are interconnected via very thin wraparound contacts and bus conductors, and, if klystrons are used for RF power conversion, series cell strings could operate at voltages up to 47.5 kilovolts.

Many solar-powered LSS in the mid to late 1980's will likely use solar cell blankets similar to these SPS candidates but will probably operate at voltages no higher than a few hundred volts.

The reference SPS demonstration article used for Grumman environmental interaction studies is shown in Figure 8. The basic planar array configuration is similar to that from a recent NASA/Boeing study, sized to provide 100 megawatts of rectified power on the ground. Structure, antenna and solar cell blankets are similar to those described above. Electrical distribution and

control networks are integrated throughout the array; power is transmitted to the antenna via slip rings. Attitude control and stationkeeping is provided by thrusters. The effective density of the spacecraft, including all subsystems is about  $3 \times 10^{-3} \text{ kg/m}^3$ .

One of many possible electrical configurations is shown in the figure. In general, solar cell strings are arranged with opposing current flow to minimize magnetic torques on the spacecraft. In this example, 16 strings each generate 250 amps at 41 to 45 kilovolts. Positive and negative busses are located at the center and ends of the array. These connect to the main power busses which run the length of the array and terminate at the slip rings. A total of 4000 amps is delivered to the RF converters at 40 kilovolts.

#### ENVIRONMENTAL INTERACTIONS AND EFFECTS

The study of LSS environmental interactions was initiated by identifying those charge/discharge effects and plasma interactions that might have an impact on the design, performance or cost of these spacecraft. Initial concerns for the SBR and SPS demonstration article are summarized in Tables 1 and 2. The potential interactions, sites and effects listed in these tables are common to most LSS using advanced solar cell arrays or phased array antennas.

Degradation of dielectric structures, optical materials and surfaces can result from repeated electrical discharges as described in the literature. Numerous dielectric-metal interfaces exist throughout the SBR and SPS, specifically at the antenna dipoles and solar cell edges, which are potentially susceptible to discharge-induced damage. Discharges on metallized dielectric delay lines and waveguides could also erode these critical elements.

Damage or disruption of the electrical distribution network, while a concern for all LSS, may be especially severe with large, distributed power systems as on SBR and SPS type spacecraft. Interactions with very high, distributed voltages and numerous RF converters and waveguide antennas are of particular importance for the SPS.

The lightweight, flexible LSS structures will distort under electrostatic forces, on-board, geomagnetic and VXB field interaction, plasma coupling currents and induced differential heating. Surface distortions and plane separation variations could have a significant effect on antenna gain, efficiency and pointing accuracy. Plasma-induced forces will also affect attitude control and stationkeeping requirements. The thrusters used for these functions may also contribute to spacecraft contamination, differential charging and power loss in multikilovolt systems.

#### ANALYSES OF LSS ENVIRONMENTAL INTERACTIONS

Preliminary analyses and engineering estimates were made to assess the possible magnitude of some of the effects of plasma interactions and other environmental factors on LSS performance. These analyses emphasized the SPS demonstration article, as it can be expected to experience such effects with

greater severity than, for example the SBR, due to its larger currents, voltages, and size.

Specifically, analyses were made of the potential distribution on the cover of a 47 KV solar array under substorm conditions and of the magnetic shielding against charging currents provided by the on-board current distributions on a 100 MW SPS demonstration article. Other estimates performed include plasma leakage currents, erosion rates due to proton scattering, torques from on-board current coupling to B<sub>GEO</sub>, and solar array performance loss due to radiation damage.

In analyzing the charging potential distribution on the 47 KV solar array an array length of 700 m was assumed, with the solar cell interconnected such as to provide a constant impressed voltage gradient along, and a constant voltage across, the array.

Without solar illumination and without the effect of solar cell cover slides, magnetic substorm charging currents would float this potential distribution so as to make most of the array length negative with respect to the plasma (based on a simple plasma particle drift approximation).

The inclusion of sun-illumination ( $J_{pe}(V_S=0) = 3 \text{ nA/cm}^2$ ) and of the effect of dielectric cover material in a self-consistent (thick sheath) analysis leads to substantially different results for the surface potential distribution on the array. The specific analyses employed the following approach: A local value of the array potential  $V_p$  is assumed and the potential  $V_S$  on the overlying surface point is calculated selfconsistently, subject to the equilibrium voltage conditions  $\sum J_i(V_S) = 0$ , where the  $J_i$  represent the current density elements shown in Fig. 9. The current balance includes the leakage current  $J_\ell$  through the dielectric cover for an appropriate value of the cover bulk resistance. The calculation is repeated for a series of equally spaced  $V_p$  values on both sides of the point where the leakage current reverses direction as a result of a change in the sign of  $(V_S - V_p)$ . The location on the array where  $V_p$  changes sign, relative to either end of the array is then determined by the condition

$$\int_{A_{in}} (J_\ell)_{in} dA = \int_{A_{out}} (J_\ell)_{out} dA$$

This also determines the parasitic current in the circuit formed through the dielectric cover, the array, and the plasma.

Two cases were analyzed, for bulk resistance values of  $10^{14}$  and  $10^{13}$  ohm-cm<sup>2</sup>, respectively. For the higher resistance, the surface potential  $V_S$  is positive but very low (a few volts), as shown in Fig. 10a. The integrated leakage current value for a 95 m wide array section is .038 amp. For the lower resistance value ( $10^{13}$  ohm-cm<sup>2</sup>) the surface potential becomes at least partly dependent on the array potential  $V_p$ . Namely,  $V_S$  becomes strongly positive for positive  $V_p$  values, while for negative  $V_p$  it remains at a few volts positive. (Fig. 10b.). The integrated leakage current here is .19 amps for the array section. Since the full array has 16 such sections the total leakage current

is 0.6 amp for the  $10^{14}$  ohm-cm<sup>2</sup> array cover and 3.1 amp for the  $10^{13}$  ohm-cm<sup>2</sup> cover. In either case this is an insignificant fraction of the 4000 amp full array current.

The SPS will produce significant magnetic fields as a result of the large array currents. These fields could act to shield the array from plasma particles, at least locally.

The effectiveness of this shielding was estimated for the 100 MW SPS demonstration article (under neglect of electrostatic forces), with current sources and current busses arranged as shown in Fig. 11. This arrangement consists of 16 sheet current sources of dimensions 190 by 377.5 meters and 14 line current sources corresponding to the current busses. Each sheet source carries a current of 250 amps, while bus currents range from 250 to 3000 amps. For this current distribution the magnetic field over the array was determined. Fig. 12 shows the component of the magnetic field  $B_{\perp}$ , lying in the plane parallel to and one meter above the array surface.<sup>11</sup> The B-field mapping provided the basis for estimating the minimum energy needed by particles to reach the array. For this estimate the particles were assumed to be normally incident on the array surface, and the minimum energy,  $E_c$ , was determined from the minimum normal momentum necessary for penetration to the distance of a gyro radius from the array surface. Values of  $E_c$  for electrons are shown in Fig. 12 at various locations on the array. For example, above the midpoint of the 3000 amp bus the array is screened from normally incident electrons of up to 32 keV. However, away from the busses, and particularly at the interfaces between opposing current sheets the electron cutoff energies for normal incidence become very low. This indicates that an arrangement of array currents, such as shown in Fig. 11, although favorable for minimizing induced torques, may promote differential charging by electrons. For protons, the cutoff energies are  $1/1836$  of those for electrons, hence, the magnetic fields considered here will not shield against protons above a few tens of electron volts. For example, the maximum proton cutoff energy, obtained above the 3000 amp bus, is 17 eV.

Another estimate concerned the torques induced from the coupling of the array currents to the ambient geomagnetic field, taken as 0.001 gauss. The array was assumed to be oriented so as to have the main current bus aligned with the field; the torques would therefore arise from forces on the secondary busses running at right angles to the main bus. A maximum torque of 18 Newton-meters (13 ft-lb) about the array center-line is estimated; the resultant increment in  $\Delta V$  requirements for attitude control is insignificant.

An estimate was also made of the added thrust capability required for station keeping if all the substorm particles were incident on only one side of the array. The combined pressure from an electron flux of  $6 \cdot 10^9$  e/cm<sup>2</sup>/sec

and a proton flux of  $1.4 \cdot 10^8$  p/cm<sup>2</sup>/sec is found to be  $7.8 \cdot 10^{-11}$  newtons/m<sup>2</sup> ( $1.6 \cdot 10^{-8}$  lb/ft<sup>2</sup>). This represents about 1/6 of the solar pressure on the array.

In view of the frequently encountered concern with ion sputtering as a mechanism for surface erosion and contaminant production, a worst case assessment of proton sputtering on SiO<sub>2</sub> was made. A continuous substorm proton flux of  $1.4 \cdot 10^8$  p/cm<sup>2</sup>/sec at kT = 15 keV was assumed, together with a spectrum-integrated sputtering yield of 10<sup>-2</sup>. This leads to a mass removal rate of  $1.4 \cdot 10^{-9}$  g/cm<sup>2</sup>/year (or  $6.3 \cdot 10^{-2}$  Å/year), which per se is insignificant; however, the optical performance of solar cell covers may be degraded in the process. The associated contaminant production rate is 0.09 g/day for the 100-MW demonstration article, which is compared with a mass release of  $1 \times 10^5$  g/day from hydrazine thrusters or  $2 \times 10^4$  g/day from cesium thrusters for station keeping.

Therefore, the development of a solar blanket in which radiation damage can be removed by on-site annealing appears to be essential for SPS. A design concept for a heat-annealable solar cell is shown in Fig. 7.

The importance of radiation damage in degrading the performance of solar arrays is well recognized. For example, radiation darkening in solar cell cover glass is expected to produce a transmission loss of ~ 4% over a 30 year SPS life-time; here the darkening tends to be limited by concurrent ultraviolet annealing. (Note that a 4% performance loss represents a 2.5% increase in SPS program costs.) By comparison, solar cell degradation by radiation is much more severe in GEO. This degradation is equivalent to that produced by a yearly fluence of 1 to  $2 \times 10^{14}$  1-MeV electrons (including the contributions from solar flares). A 16% efficient cell will degrade 20 to 30% over 10 years in GEO, primarily due to solar flare proton damage.

#### LARGE SCALE ENVIRONMENTAL INTERACTION EXPERIMENT PLATFORM

Air Force and NASA studies are now defining test articles and flight programs which will demonstrate on-orbit construction of large space structures. These demonstrations will be the first LSS-related activities in space, and according to current plans, will occur by 1984. One of the concepts for such a demonstration article is shown in Figure 13. This utility platform is constructed while attached to the Shuttle, utilizing one-meter beams which are fabricated by the automatic beam builder located in the Shuttle payload bay. A simple gravity-gradient stabilized platform is shown in the figure which supports several earth-pointing experiments. Electrical power and other subsystems have also been added to provide long-term, free flyer capability.

The same platform could carry a variety of material, component and subsystem segments as depicted in Figure 14. In this example, several different material, solar cell blanket and antenna gore samples, in various sizes and configurations, are mounted over almost all of the available 900 square meter test surface. Temperature and illumination sensors, particle and electromagnetic pulse (EMP) detectors are distributed throughout the test samples.

Integrators, recorders and other equipment are located in an experiment support package. The platform is powered by radioisotope thermoelectric generator (RTG) to eliminate plasma disturbances and orientation requirements associated with solar cell arrays.

#### Low Earth Orbit (LEO) Tests

The platform can be left in LEO for extended periods and periodically revisited by the Shuttle. Test samples and on-board data can be retrieved, and new samples added if desired.

Since LEO plasma characteristics are significantly different from those in geosynchronous orbit (GEO), relatively few LEO test results will extrapolate to GEO. However, charge/discharge effects, passive charge controls and space environment synergisms could be evaluated, and size/configuration relationships established for large area elements. Also, since most LSS programs include construction and operation of demonstration systems in LEO, these tests will provide valuable design/performance data for these systems.

Other tests which might be used to verify analytical models and ground test results are

- Materials response-plasma dynamics
- Transient-induced differential charging
- Discharge avalanche
- Electric/magnetic field-induced forces
- Voltage/leakage current scaling

#### High Altitude Tests

With the addition of a propulsion stage, the platform could be placed in elliptical orbit or in GEO where the majority of LSS will eventually operate. A conceptual design of the largest test platform which could be boosted to high altitude from LEO is shown in Figure 15. This article is constructed in a manner identical to that described above, with its maximum dimensions nearly 100 meters. A cluster of three IUS (Interim Upper Stage) engines are used to propel the 6800 kilogram spacecraft. A total of 4800 square meters of platform area is available for test samples. Instrumentation and experiment support equipment is distributed throughout the platform, and an RTG used for electrical power as with the LEO platform. One or more retractable plasma probes can be added as shown to measure plasma characteristics at various distances from the spacecraft. Motor-driven boom designs are available for probe extensions up to one kilometer.

A test platform of this type in GEO could provide definitive environmental interaction data to guide the design of future LSS. The following types of

tests could be performed, in addition to those listed above, for a nearly complete characterization of physical processes and coupling mechanisms:

- Electric field acceleration
- Magnetic field deflection/focusing
- Plasma-induced heating
- Geometrical particle shadowing
- Plasma sheath formation
- Plasma instability non-linear effects
- Spacecraft geomagnetic wake
- Active charge controls
- Large scale performance verification

This LSS test platform could be constructed and placed in GEO by the mid-1980's. Real-time data could be recorded shortly after orbit insertion. Data can be sampled over long intervals to evaluate effects of environment variations and long-term material property changes.

An advanced orbit transfer vehicle (OTV), which might be available around 1990, could visit the LSS test platform in GEO. Test samples could be inspected, retrieved for ground tests and replaced with new or different samples for additional space testing. If accelerated materials ground tests cannot be properly developed, or prove too costly, long-term GEO experiments of this type may be the only way to derive the design data and confidence levels needed before committing to development of a complex, costly LSS.

Much research and engineering analysis must yet be done to estimate LSS environmental interactions and effects. Many plasma-related interactions and long-term materials effects will most likely require large test articles of the type described above; the opportunity to fly these experiments will be here shortly. A program should be formulated now to define the research and analyses to be performed, the types of experiments to be flown, and to begin preliminary designs of the large scale experiment platform.

**TABLE 1 POTENTIAL CHARGE/DISCHARGE EFFECTS ON LSS**

EFFECT	SBR	SPS DEMO
● DIELECTRIC CRAZING/DARKENING	● SOLAR CELL COVERS & THERMAL CONTROL SURFACES	
● DIELECTRIC EMBRITTLEMENT	● SOLAR ARRAY SUBSTRATE & COMPOSITE/GLASS ➤ STRUCTURAL ELEMENTS	
● CONTAMINANT DEPOSITION	● SOLAR CELL COVERS, THERMAL CONTROL SURFACES ● ACCELERATED ELECTRICAL DISCHARGES	
● METAL EROSION/VAPORIZATION	● SOLAR CELL INTERCONNECTS & THERMAL BLANKETS	
	● ANTENNA DIPOLES/DELAY LINES/ELECTRONIC MODULE CONTACTS	● METAL/COMPOSITE WAVEGUIDES
● INSULATION BURNTHROUGH	● DC POWER DISTRIBUTION	
		● RF CONVERTER FEEDS
● EMI/VOLTAGE TRANSIENTS	● SUBSYSTEM WIRING/ELECTRONICS	
	● ANTENNA POWER DISTRI- BUTION & ELECTRONICS	● POWER DISTRIBUTION NETWORK
● ELECTROSTATIC FORCES- STRUCTURAL DISTORTIONS	● PRIMARY/SECONDARY STRUCTURE	
	● ANTENNA/GROUND PLANES	

**TABLE 2 POTENTIAL PLASMA INTERACTIONS WITH LSS**

INTERACTION	SBR	SPS DEMO
● PLASMA PARTICLE ACCELER- ATION BY CHARGED SURFACES	● INCREASED RADIATION DAMAGE ● ORBIT/ATTITUDE DISTURBANCE FORCES	
● PLASMA/LSS COUPLING CURRENTS	● EXAGGERATED ECLIPSE/LOAD TRANSIENTS ● DISTORTING FORCES/TORQUES	
● MAGNETIC FIELD FOCUSING/ DEFLECTION	● INCREASED DIFFERENTIAL CHARGING	
	● ANTENNA POWER DISTRIB.	● POWER DISTRIB. NETWORK
● ELECTRIC FIELD ACCELERATION		● AVALANCHE BREAKDOWN
● PLASMA LEAKAGE CURRENTS		● HIGH VOLTAGE POWER LOSS
● ELECTRIC/MAGNETIC FIELDS - ELECTRON BEAMS		● RF CONVERTER BEAM DEFOCUSING
● MULTIPACTOR DISCHARGE		● WAVEGUIDE BREAKDOWN
● ION THRUSTER EXCHANGE CURRENTS	● INCREASED DIFFERENTIAL CHARGING	
		● INCREASED POWER LOSS

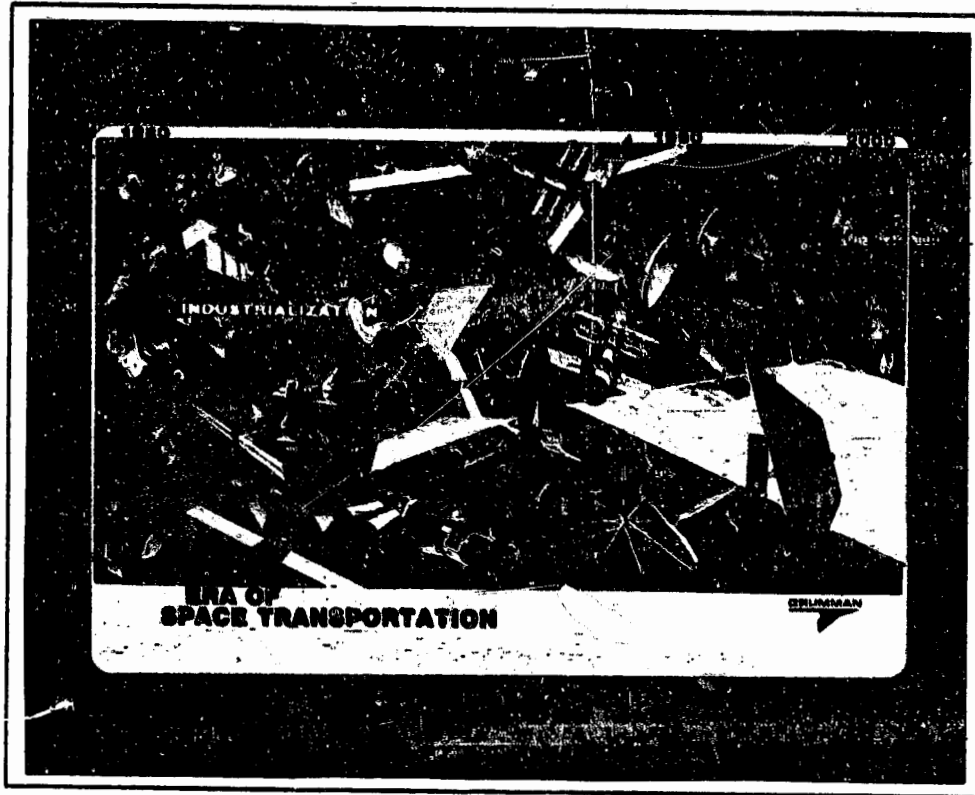


Figure 1. Era of Space Transportation

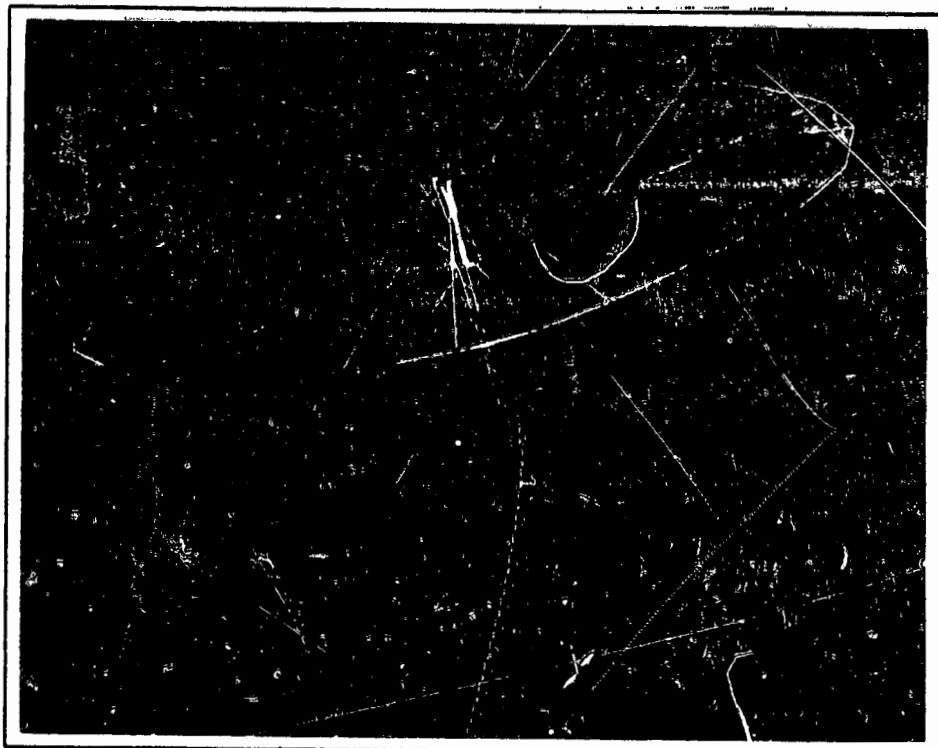


Figure 2 Space Based Radar Configuration

ORIGINAL PAGE IS  
OF POOR QUALITY

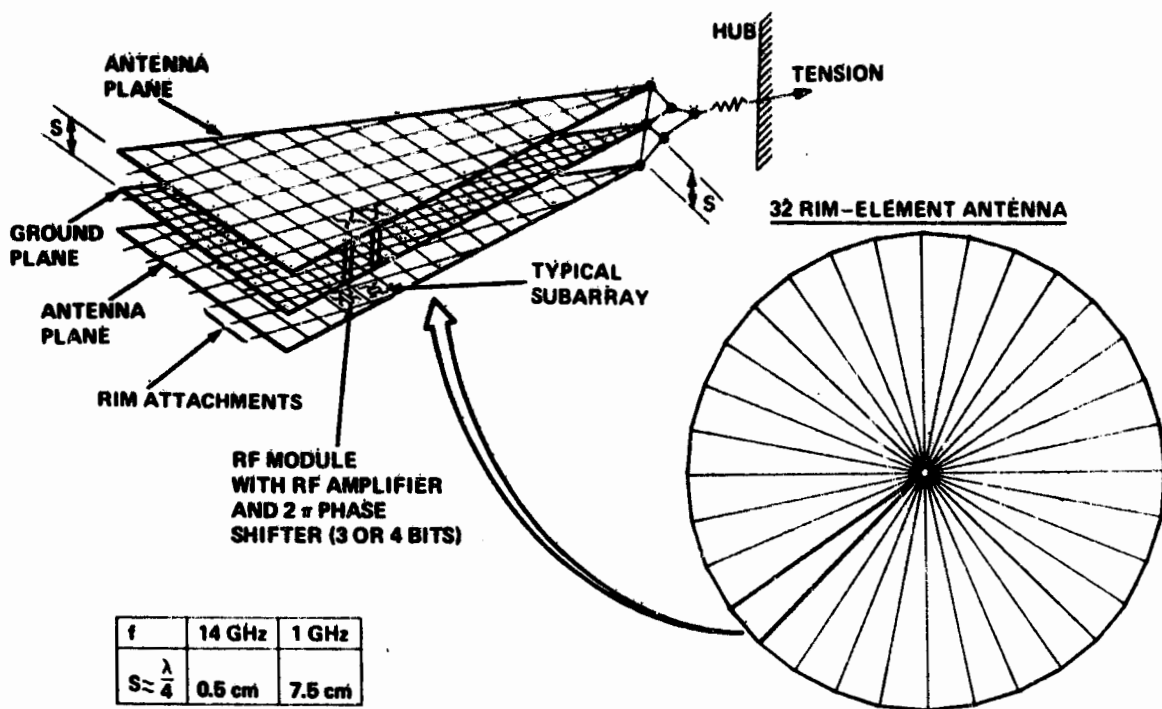


Figure 3. Phased Array (Active)

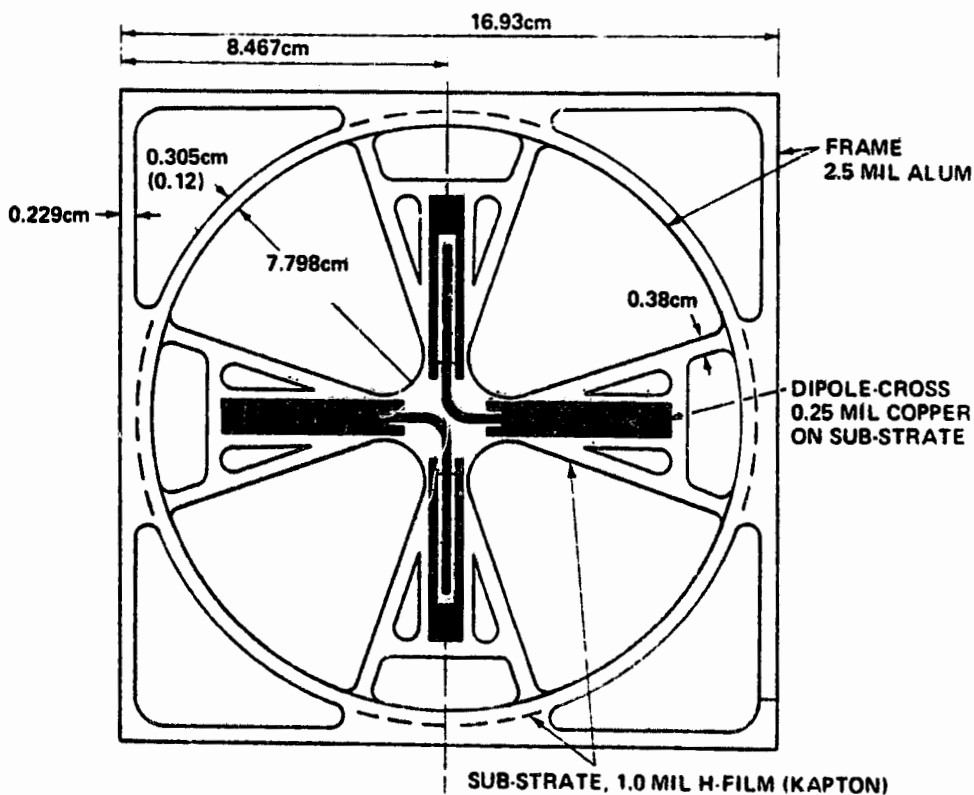
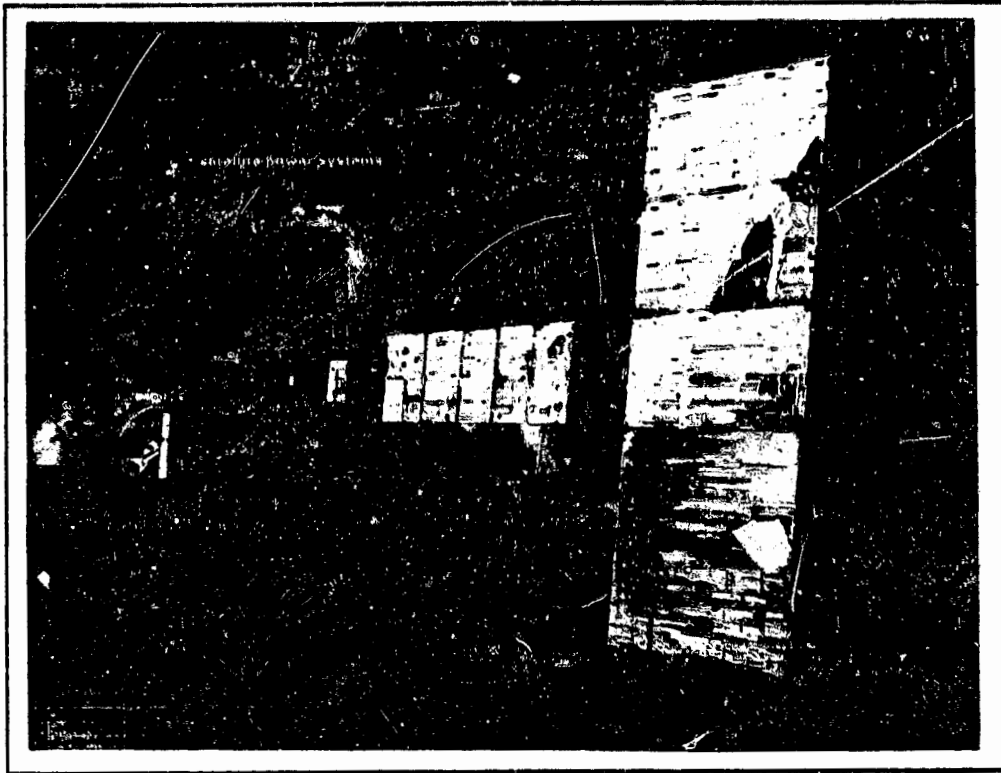
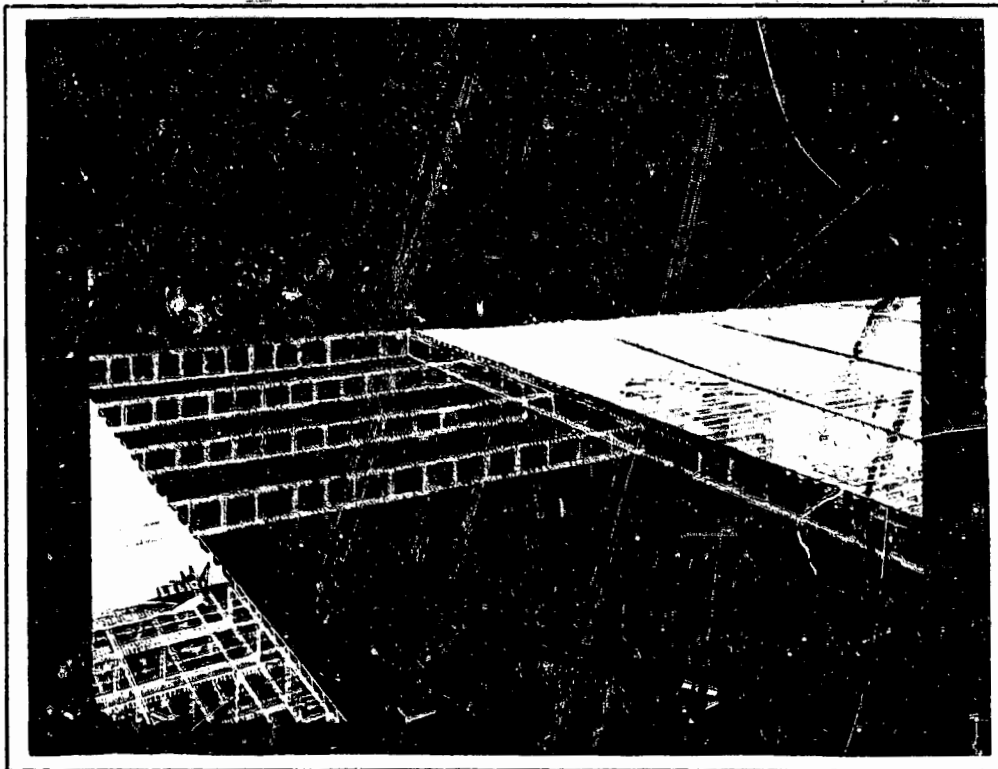


Figure 4. Subarray Structural Arrangement

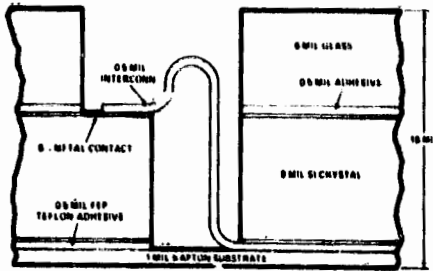


**Figure 5. Evolution of Solar Satellite Power Systems**

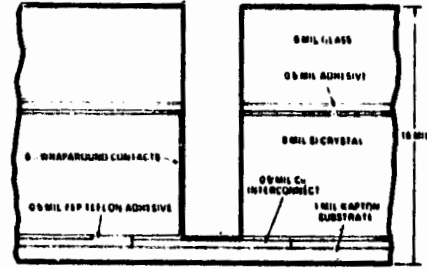


**Figure 6. SPS Construction (Antenna Proximity)**

TODAY'S TECHNOLOGY



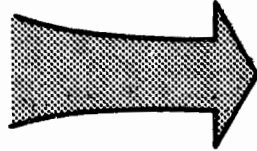
STATE-OF-ART ARRAY - EARLY 70's



BASELINE SEPS ARRAY

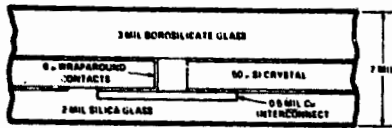
ISSUES TO BE RESOLVED

- MATERIALS SELECTION
- LONG TERM ENVIR. EFFECTS
- DESIGN

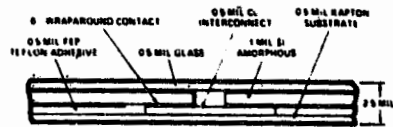


PRODUCIBILITY  
• AUTOMATED BLANKET FABRICATION

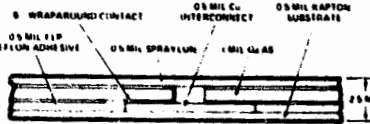
SPS CANDIDATES



SILICON CRYSTAL (ANNEALABLE)



SILICON AMORPHOUS



GALLIUM ARSENIDE CRYSTAL

Figure 7. Solar Blanket

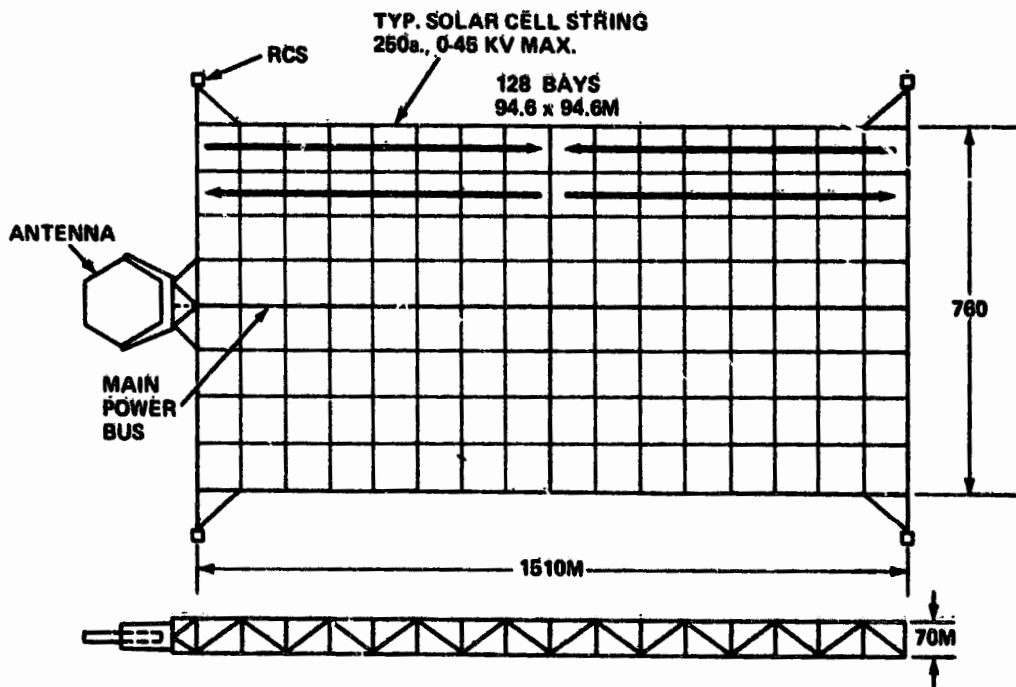


Figure 8. 100-MW SPS Demo Reference Electrical Configuration

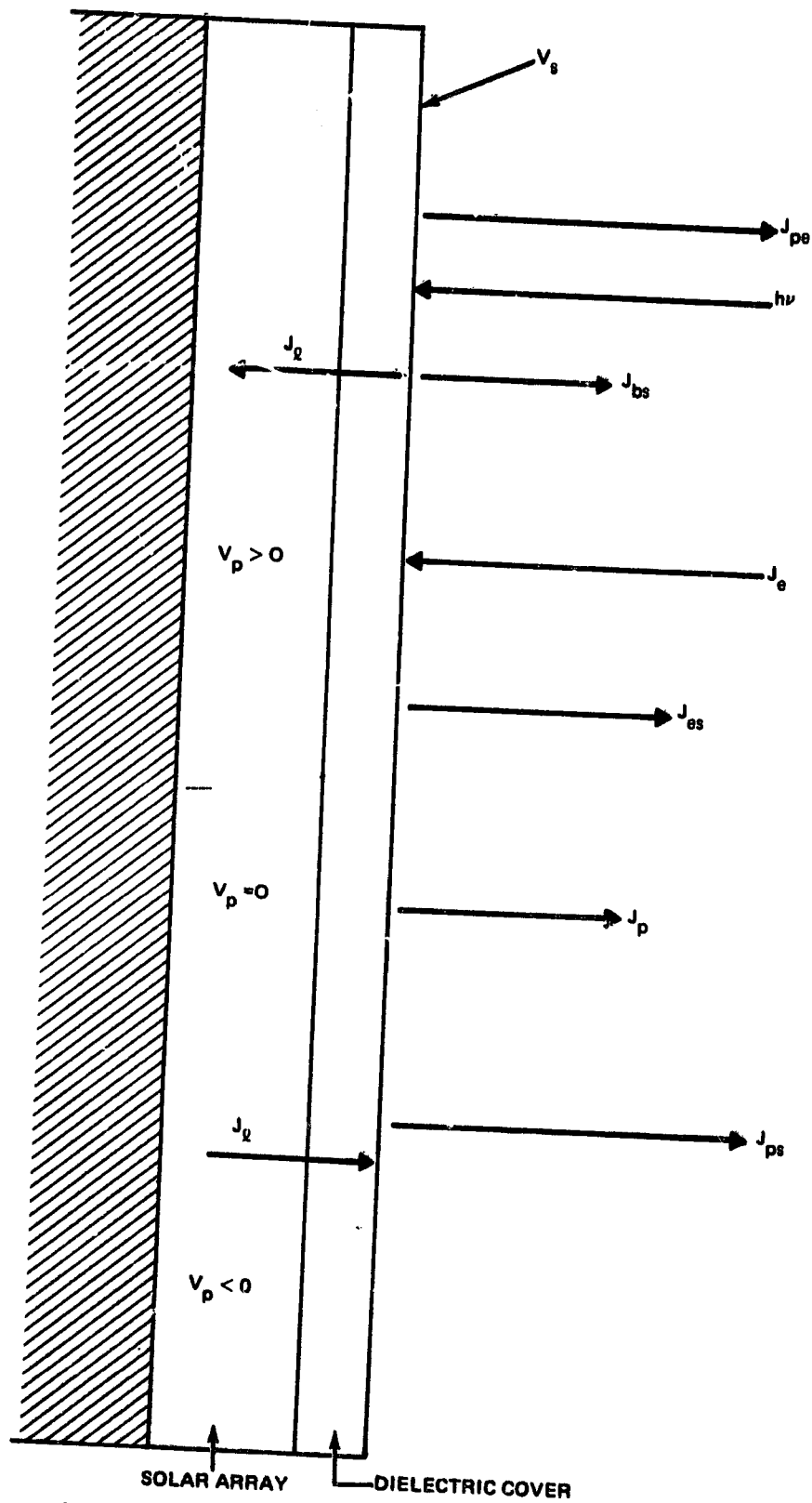


Fig. 9 Charging Currents on Solar Array with Dielectric Cover

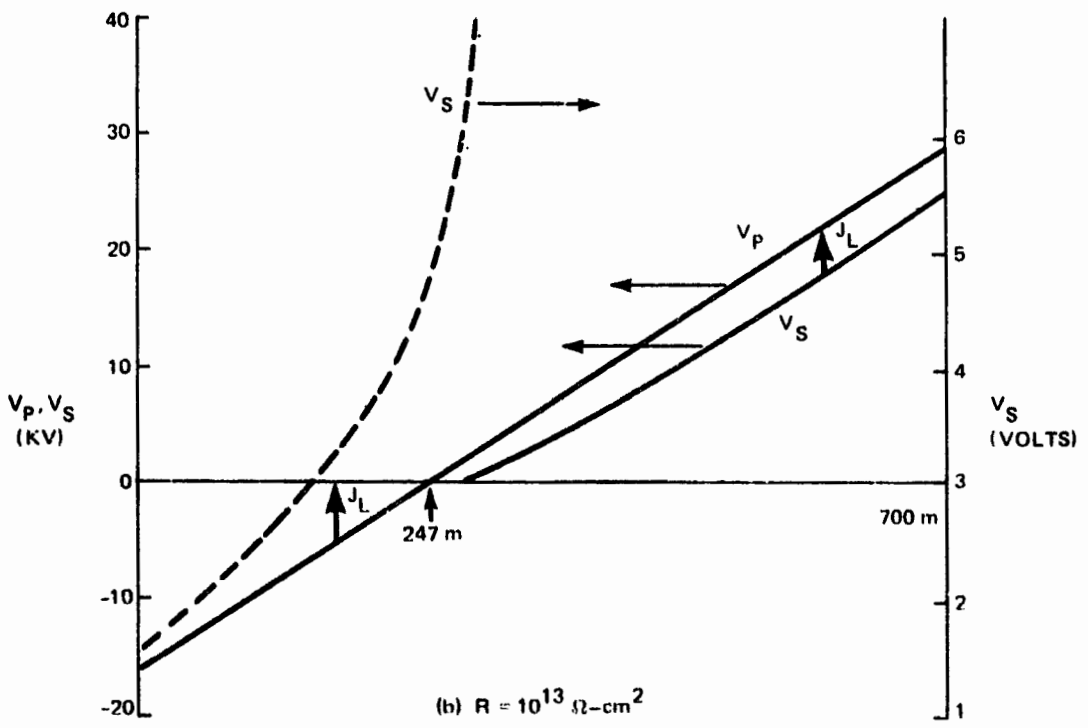
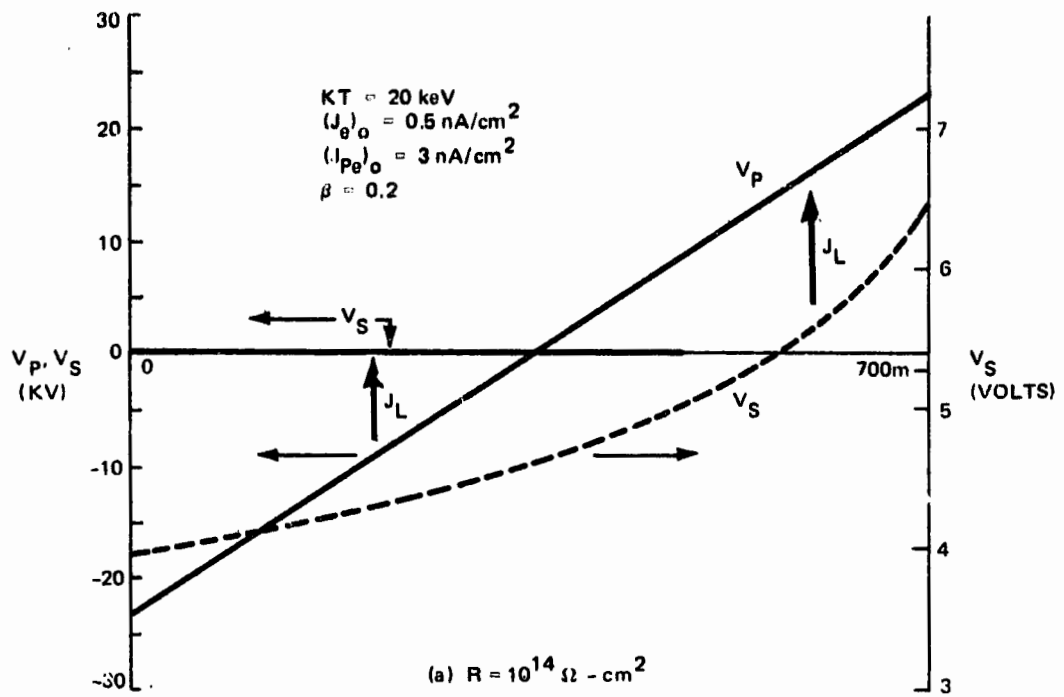


Fig. 10 Surface Potential ( $V_S$ ) and Solar Cell Floating Potential ( $V_P$ ) for 47-KV Solar Array with Cover

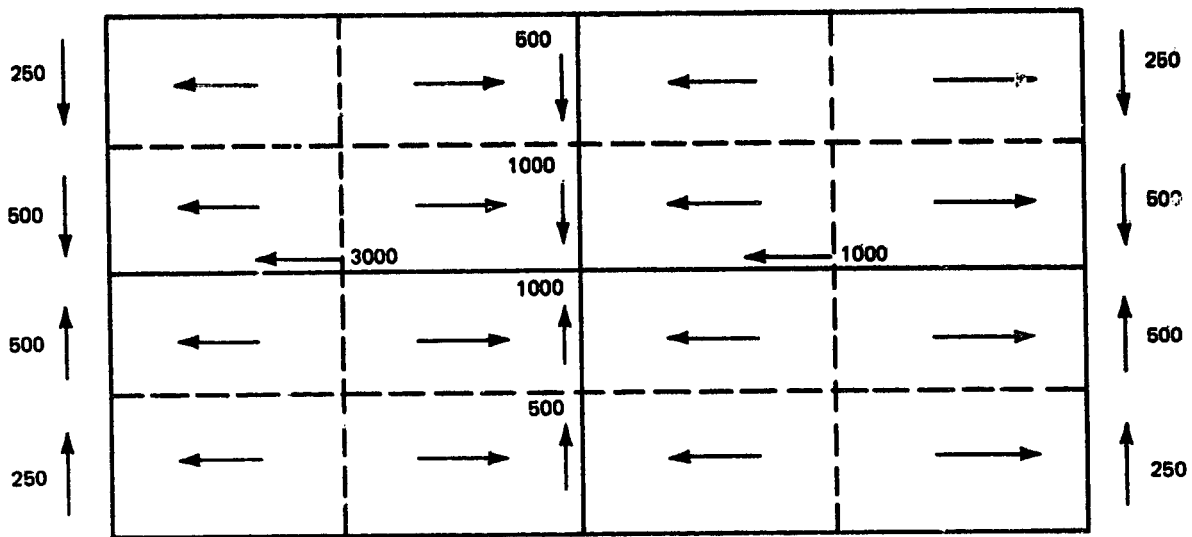
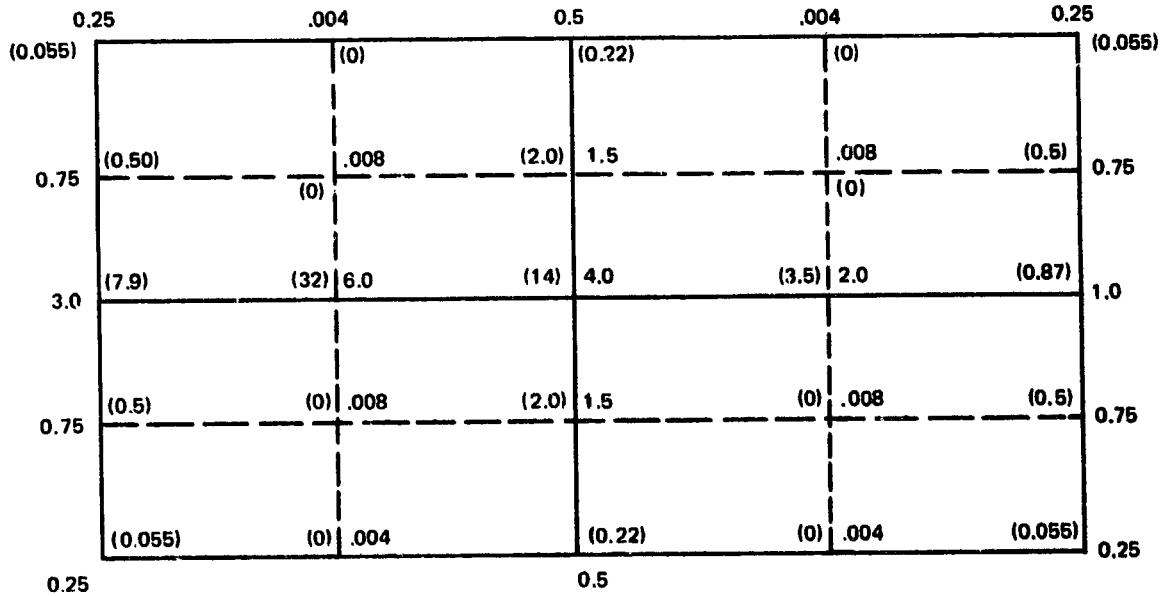


Figure 11. SPS Current Flow



B PARALLEL (GAUSS) AT 1m ABOVE ARRAY SURFACE:  
 ( ) =  $E_c$  (KeV) (ELECTRONS)

Figure 12. SPS Magnetic Shielding

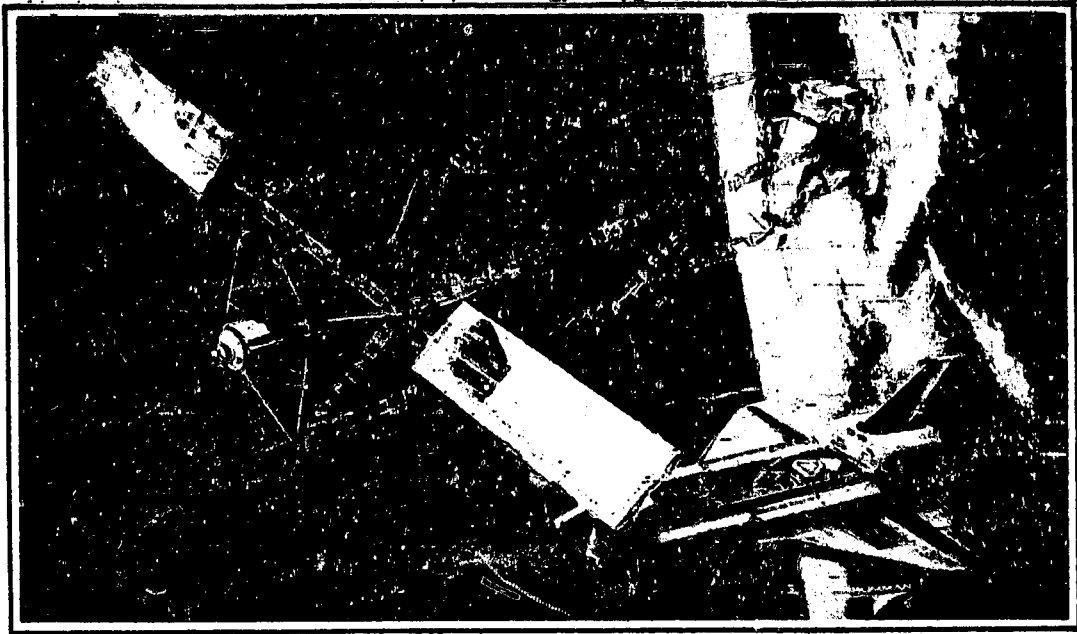


Figure 13. Utility Platform Constructed by Shuttle-Based Beam Builder

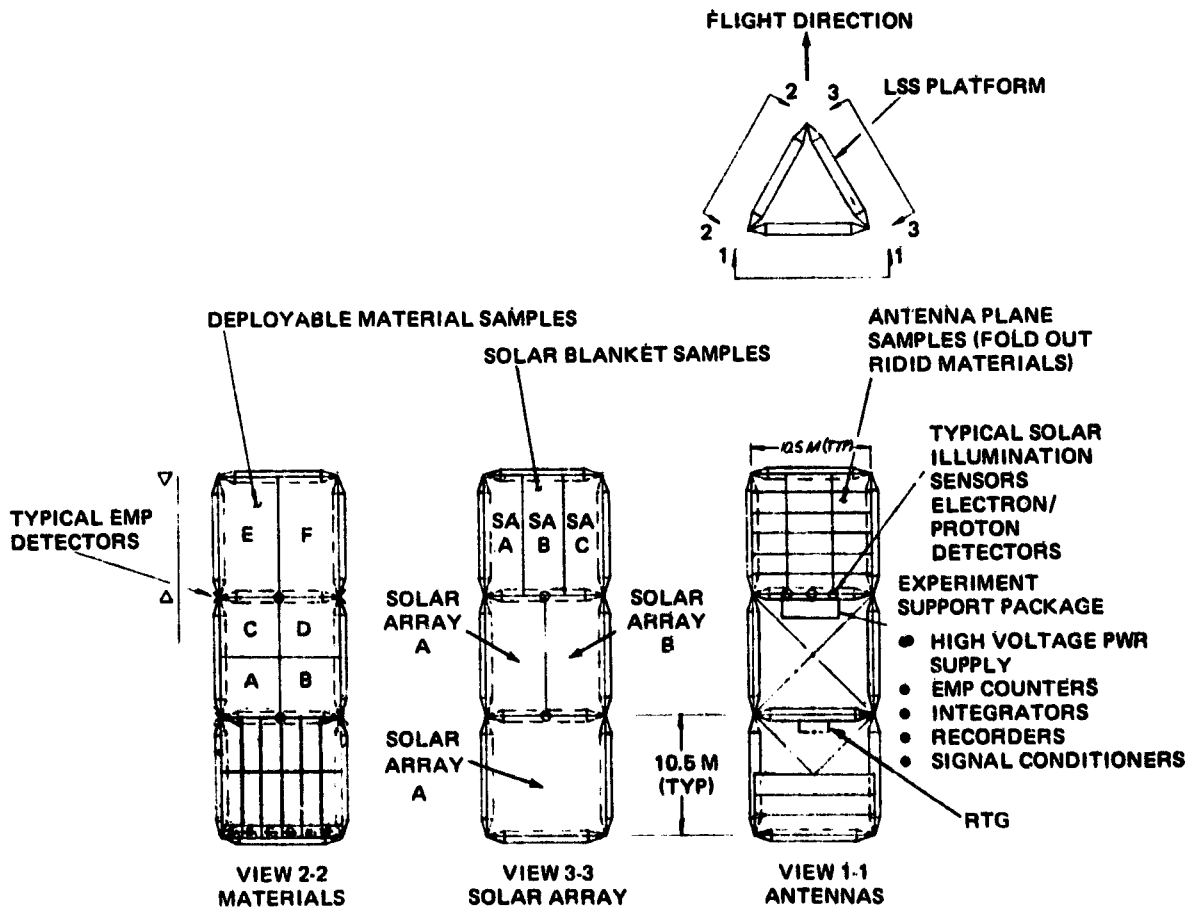


Figure 14. Materials Exposure/Plasma Charging Experiment

407

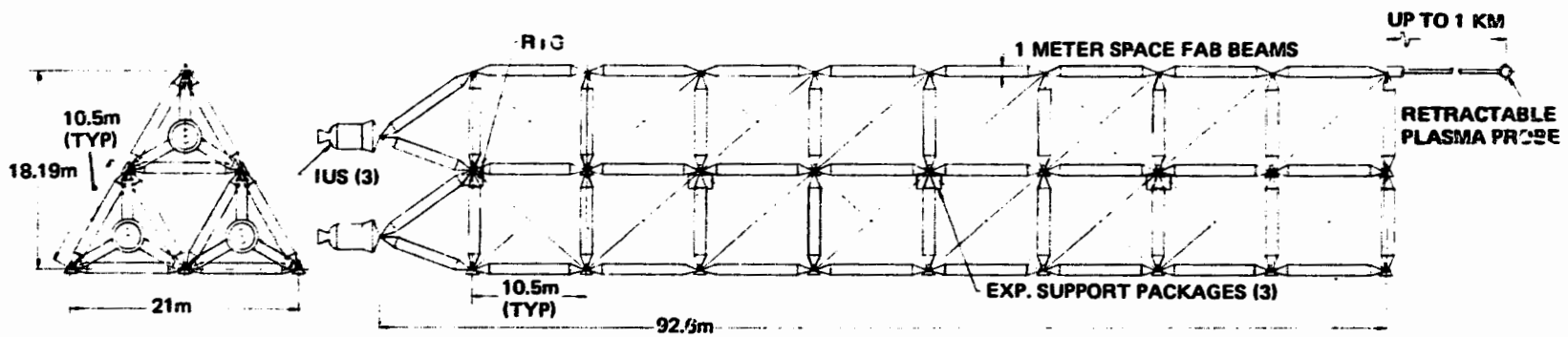


Figure 15. Large Scale GEO Exp. Platform